Proton wires in an electric field: the impact of the Grotthuss mechanism on charge translocation

2003 J. Phys.: Condens. Matter 15 291

(http://iopscience.iop.org/0953-8984/15/2/329)

INSTITUTE OF PHYSICS PUBLISHING JOURNAL OF PHYSICS: CONDENSED MATTER

J. Phys.: Condens. Matter **15** (2003) 291–307 PII: S0953-8984(03)52821-1

Proton wires in an electric field: the impact of the Grotthuss mechanism on charge translocation

Natalie Pavlenko[1]

Institute for Condensed Matter Physics, 1 Svientsitsky Street, UA-79011, Lviv, Ukraine

E-mail: natalie@physik.tu-muenchen.de

Received 29 August 2002
Published 20 December 2002
Online at stacks.iop.org/JPhysCM/15/291

Abstract

We present the results of the modelling of proton translocation in finite H-bonded chains in the framework of the two-stage proton transport model. We explore the influence of reorientation motion of protons, as well as the effect of electric field and proton correlations on system dynamics. An increase of the reorientation energy results in the transition of proton charge from the surrounding to the inner water molecules in the chain. Proton migration along the chain in an external electric field has a steplike character, proceeding with the occurrence of electric field threshold-type effects and drastic redistribution of proton charge. Electric field applied to correlated chains induces first a formation of ordered dipole structures for lower field strength, and then, with a further field strength increase, a stabilization of states with Bjerrum D-defects. We analyse the main factors responsible for the formation/annihilation of Bjerrum defects showing the strong influence of the complex interplay between reorientation energy, electric field and temperature in the dynamics of the proton wire.

1. Introduction

Translocation of protons over long distances has a key importance for biological and chemical systems. It is believed that proton migration along the chains of water molecules formed between the interior of proteins and the solvent establishes electrochemical potential gradients playing an important functional role [1, 2]. Experimental evidence indicates that the dominant mechanism responsible for proton transport in transmembrane proteins (for instance, in bacteriorhodopsin of *Halobacterium halobium* [3, 4] and in gramicidin A channels [4, 5]) is the diffusion of H^+ ions which is faster than the hydrodynamic flow of hydronium species $(H_3O)^+$. Especially at low hydrogen concentrations in channels, proton conduction is determined by a two-stage Grotthuss-type mechanism [6, 7] shown schematically in figure 1(a). The first

[1] Present address: Institut für Theoretische Physik, Physik-Department der TU München, James-Franck-Strasse, D-85747 Garching b. München, Germany.

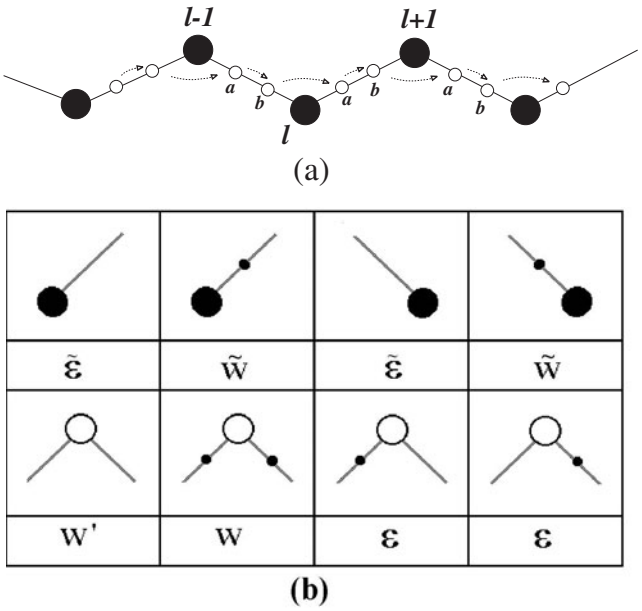

Figure 1. (a) Schematic presentation of proton wire; arrows indicate a possible path of proton migration along the chain. Full circles denote water molecules and open circles are the possible positions for excess protons. (b) Scheme of possible proton configurations near the outer surrounding groups (the upper part) and the inner water molecules of the wire (the lower part).

stage involves the intrabond proton tunnelling along the hydrogen bridge which is connected with the formation and transfer of ionic positive (H_3O^+) and negative (OH^-) charged defects. To sustain a flux of H^+ in such a proton wire, the inter-molecular proton transfer due to the reorientations of molecular groups with protons is assumed. Reorientation motion leads to the breaking of the hydrogen bond (the so-called orientational Bjerrum L-defect) and location of the proton between another pair of molecular groups [8]. Consequently, the reorientation step in the presence of the second proton may induce a high-energy configuration with both of the protons shared by two adjacent oxygen ions (Bjerrum D-defect).

Unlike the translocation of monovalent ions like Cs^+, Na^+ or K^+ via gramicidin requiring the net diffusion of the whole water column in the channel, the existence of the Grotthuss-type selective migration of H^+ through the H-bonded chain is supported by the absence of streaming potentials during H^+ permeation [5, 9]. In contrast to bulk water, the reorientation motion in a one-dimensional water wire involving a migration of Bjerrum defects with the period of reorientations about 10^{-10} s is much slower than the proton intra-bond hopping ($\sim 10^{-12}$ s) [10, 11]. This is also closely related to the fact that the mobility of Bjerrum defects ($\sim 10^{-4}$ cm^3 V^{-1} s^{-1}) is much lower than that of ionic defects ($\sim 10^{-2}$ cm^3 V^{-1} s^{-1}) [12]. Moreover, as appears from the results of molecular dynamics simulations [14], the translocation of the ionic defects in proton wires is an almost activationless process, whereas the orientation defects involving an activation energy of about 5 kcal mol^{-1} in the chain containing eight water molecules constitute a limiting step for the proton migration. Besides the orientation defects, the recent experiments indicate that another possible rate-limiting step for the proton migration in gramicidin channels can be at the membrane-channel/solution interface [11, 13].

As was pointed in [6], the experimental analysis of the proton flow in bioenergetic proteins and the mechanism of proton translocation is very difficult because of its intrinsically transient

nature. To shed more light on the microscopic nature of the proton transport and to analyse the influence of quantum effects and interaction with proton surroundings, theoretical modelling remains essentially important. Recently, much attention has been focused on the theoretical studies of the dynamics of ionic defects using soliton models [15, 16] and molecular dynamics simulations [17–20]. Proton transfer in water was shown to be strongly coupled with the dynamics of the local environment, and the density of ionic defects was found to increase exponentially with increasing temperature [15]. However, since the concentration of slow Bjerrum defects in water solutions is much higher ($c_B = 2 \times 10^{-7}$ at $-10\,^{\circ}$C) than that of fast ionic defects ($c_I = 3 \times 10^{-12}$) [12], investigations of the reorientation step of proton migration are necessary for better understanding of the proton transport process.

The goal of the present work is to study a proton wire containing a finite number of water molecules by the use of quantum statistical mechanics methods which are extremely effective in the description of the collective nature of the proton transfer and in the quantum treatment of the light H nuclei [21]. To describe correctly the proton transport process, we employ here a two-stage proton transport model [22] incorporating quantum effects such as proton tunnelling and zero-point vibration energy. In earlier papers [23–25] we applied the two-stage model to analyse the effect of coupling between protons and molecular group vibrations on proton conductivity in infinite H-bonded chains and proton-conducting planes. In particular, it was shown that the proton–lattice vibration interactions induce structural instabilities and charge ordering in a system [23], whereas the Grotthuss-type transport mechanism manifests itself in nontrivial temperature and frequency dependences of the proton conductivity [24–26].

In this work we analyse the influence of proton–proton correlations, comparing two different protonated chains containing one and two excess protons respectively. We find that the reaction of protonation of a water chain is extremely sensitive to the reorientation energy barrier of proton motion and the barrier for the chain protonation. We show that the increase of the reorientation energy results in the drastic decrease of the proton charge density at the boundary between the chain and its surroundings with consequent localization of protons near the inner water molecules. As appears from our modelling, the application of external electric field induces the steplike threshold-type effects with the ordering of proton charge and stabilization of Bjerrum D-defects in the wire. We analyse the temperature dependence of proton polarization and D-defect concentration, and examine the role of the interplay between different factors (such as orientation energy, external field and temperature) in the dynamics of Bjerrum defects.

2. Model specification and method of calculation

To model a proton wire, we consider a linear chain containing N hydrogen bonds and $l = 1, 2, \ldots, N, N+1$ molecular groups. The outer left ($l = 1$) and right ($l = N+1$) molecular complexes mimic the surroundings of the proton wire and differ from the inner ($l = 2, \ldots, N$) water molecules. The transport of an excess proton through the wire proceeds via the following two steps:

(i) the proton can be transferred within a H bond (process shown by short arrows in figure 1(a)) which is modelled by a simple double-well potential, with the corresponding energy barrier Ω_T for the proton transfer between the two minima,

$$H_T = \Omega_T \sum_{l=1}^{N} (c_{la}^{+} c_{lb} + c_{lb}^{+} c_{la}), \tag{1}$$

where $c_{l\nu}^{+}$ ($c_{l\nu}$) are the operators of the proton creation (annihilation) in the position (l, ν) (the index $\nu = \{a, b\}$ denotes the left/right position for the proton within the H bond);

(ii) a water molecule together with a covalently bonded hydrogen ion can be rotated, and this process causes the breaking of the H bond and location of H^+ between another two nearest water molecules of the wire (process depicted by long arrows in figure 1(a)),

$$H_R = \Omega_R \sum_{l=1}^{N} (c^+_{l+1,a} c_{lb} + c^+_{lb} c_{l+1,a}), \tag{2}$$

where Ω_R is the effective energy barrier for the proton hopping between the states $|l+1, a\rangle$ and $|l, b\rangle$ (reorientation of the lth molecular group together with the proton). As is shown in [27] by the computation of the proton mean-force potential, this transition between donor–acceptor and acceptor–donor states reverses the chain dipole moment and requires a substantial energy barrier of about 5.5 kcal mol^{-1} for the whole chain containing up to eight water molecules. Besides the transport process, we incorporate the following two types of interaction between protons in the chain.

(iii) Different short-range configurations of the protons near an inner water molecule as well as an outer molecular group can appear due to the different nature of bonding (shorter covalent or longer H bond). The energies of possible configurations (shown in figure 1(b)) are described by the following terms:

$$\begin{aligned} &H_1 = \tilde{\varepsilon}_1(1 - n_{1a}) + \tilde{w}_1 n_{1a}, \qquad H_{N+1} = \tilde{\varepsilon}_{N+1}(1 - n_{Nb}) + \tilde{w}_{N+1} n_{Nb}, \\ &H_l = w'(1 - n_{l+1,a})(1 - n_{lb}) + w n_{l+1,a} n_{lb} + \varepsilon(1 - n_{lb}) n_{l+1,a} + \varepsilon n_{lb}(1 - n_{l+1,a}). \end{aligned} \tag{3}$$

The parts H_1 and H_{N+1} describe the energies of the boundary proton configurations near the left- and the right-hand surrounding molecular groups (we assume for simplicity $\tilde{\varepsilon}_1 = \tilde{\varepsilon}_{N+1} = \tilde{\varepsilon}$ and $\tilde{w}_1 = \tilde{w}_{N+1} = \tilde{w}$ in the boundary configurations shown in the upper scheme of figure 1(b)). The terms H_l ($l = 2, \ldots, N$) contain the configuration energies for the water molecules in the interior of the wire (the lower part in figure 1(b)). Here the proton occupancy operators $n_{l\nu} = c^+_{l\nu} c_{l\nu} = \{0, 1\}$.

(iv) A strong repulsion between two nearest protons shared by two neighbouring oxygens (so called Bjerrum D-defect) with a repulsion energy U is represented by the term

$$H_C = U \sum_{l=1}^{N} n_{la} n_{lb}. \tag{4}$$

In our following analysis we use the value of $U \approx 10$ kcal mol^{-1} corresponding to the energy of a relaxed D-defect estimated in [28] on the basis of quantum chemical calculations.

To model a field exerted by the surroundings, we apply an external electric field of strength E to the proton wire, which is described by the following term:

$$-e_p E \sum_{\substack{l=1 \\ \nu=\{a,b\}}}^{N} R_{l\nu} n_{l\nu}, \tag{5}$$

where $R_{l\nu}$ is the coordinate of the proton position (l, ν) with respect to the centre of the chain, and e_p denotes the proton charge.

In order to analyse the dynamics of the proton wire embedded in the surroundings under the influence of the field, as well as the effect of rotational motions of covalent groups with protons, we will focus our attention on the polarization of the proton wire defined here as

$$P = e_p \sum_{\substack{l=1 \\ \nu=\{a,b\}}}^{N} R_{l\nu}\langle n_{l\nu}\rangle, \tag{6}$$

where $\langle\cdots\rangle$ denotes the statistical average with respect to the system energy (1)–(5). The average probabilities $\langle n_{l\nu}\rangle$ of occupation of the position $(l,\ \nu)$ by the proton describe the distribution of the proton charge in the wire, and thus are another very important characteristic to track the proton migration.

To calculate *exactly* the above-mentioned statistical averages, we need to know the quantum energy levels determined by the energy (1)–(5). This can be done by a mapping of the proton states $(l,\ \nu)$ on the multi-site basis $|i\rangle = |n_{1a}, n_{1b}, \ldots, n_{Nb}\rangle$. Then, using the projection operators $X^{ii'} = |i\rangle\langle i'|$ acting on the new basis $|i\rangle$ we rewrite the system energy (1)–(5) in a convenient form (see the appendix):

$$H = H^0 \oplus H^1 \oplus \cdots \oplus H^{2N}. \tag{7}$$

Each term H^{n_p} in (7) corresponds exactly to n_p protons in the chain ($n_p = \sum_{l,\nu}\langle n_{l\nu}\rangle = 0, 1, \ldots, 2N$). This means in fact that the mapping on the states $|i\rangle$ allows us to decompose the terms (1)–(5) and analyse the cases of different numbers of protons in the wire separately.

The energy barrier for the protonation of the chain is described by the parameter Δ which appears in (7) after the decomposition procedure (see the appendix). As follows from the definition (A.8), Δ is the difference between the energies of the proton attraction to the boundary and to the inner water molecules. As the PMF studies of the H-bonded chain dynamics [27] show that the inner H bonds are stronger (shorter O–O separation distances) than the outer H bonds, it is reasonable to consider below the case $\Delta < 0$ (we take $|\Delta| = 0.85$ kcal mol^{-1} in our numerical calculations), when the proton is attracted to the surroundings and needs to overcome the boundary energy barrier $|\Delta|$ to protonate the water chain.

The parameter $J = w + w' - 2\varepsilon$ (see figure 1(b)) is related to the effective short-range interactions between the protons near the water molecule. It describes, in fact, the energy of the formation of the pair of ionic defects: $\mathrm{I}_+ = \mathrm{H_3O^+}$ $(w - \varepsilon)$ and $\mathrm{I}_- = \mathrm{OH^-}$ $(\varepsilon - w')$ from two water molecules in the dissociation reaction ($2\mathrm{H_2O} \rightarrow \mathrm{H_3O^+} + \mathrm{OH^-}$). Since the value of J is about 22 kcal mol^{-1} [12, 30] and is more than twice U, we exclude in our following analysis the appearance of the pair of ionic defects in the system.

Due to the two types of motion we have two different contributions to the proton dipole moment: the orientational part $\mu_r = e_p R_r$ and the transfer part $\mu_{ab} = e_p R_{ab}$ where $R_{ab} = R_{lb} - R_{la}$ denotes the distance H–H between the two nearest proton positions of the double-well H bond. In our calculations, we use the values $\mu_{ab} = 3.5$ and $\mu_r = 4.5$ D corresponding to the moderately strong H bond with an O–O distance $R_{ab} + 2R_r = 2.6$ Å and the covalent O–H bond of length $R_r = 0.94$ Å.

3. Case study: one excess proton in chain

As the starting point, in this section we mimic the situation when one proton is moved towards the water chain embedded into the solvent. To examine the behaviour of the protonated chain with N H bonds and $n = 1$ excess proton, we consider the H^1 part of the energy given by (A.4). Since the zero-point vibration energy for protonated chains is larger than the potential energy barrier for the proton transfer between two shared oxygens [31], quantum tunnelling is not required for the intra-bond $\mathrm{H^+}$ transfer. Thus, in our modelling we set $\Omega_T \approx 0$. With this

assumption, the energy levels of H^1 can be found *exactly*:

$$\lambda_{1,2} = \Delta \pm \left((N-1)\mu_r + \frac{N}{2}\mu_{ab}\right)E,$$

$$\lambda_{3,\ldots,2N} = \begin{cases} \pm\mathrm{i}\left(\dfrac{\mu_{ab}}{2} + \mu_r\right)E \pm p & (i = 1, 3, \ldots, N-2), \text{ for odd } N \\ \pm\mathrm{i}\left(\dfrac{\mu_{ab}}{2} + \mu_r\right)E \pm p & (i = 0, 2, \ldots, N-2), \text{ for even } N \end{cases} \tag{8}$$

where $p = \sqrt{\mu_r^2 E^2 + \Omega_R^2}$.

To analyse the role of Ω_R we consider first the case without external field ($E = 0$). Depending on the value of Ω_R, two different regimes may be stabilized in the system. In the first *small-Ω_R regime*, the two lowest energy levels $\lambda_{1,2}$ correspond to the superposition of the two boundary states

$$|10\ldots00\rangle \qquad \text{and} \qquad |00\ldots01\rangle \tag{9}$$

with the proton located in the surroundings near the left-or the right-hand outer molecular groups. In the second *large-Ω_R regime* the proton is shared between the inner water molecules of the chain and the ground state of the system corresponds to the superposition of the states

$$|010\ldots00\rangle, |0010\ldots00\rangle, \ldots, |00\ldots010\rangle \tag{10}$$

with the energies $\lambda_4, \lambda_6, \ldots, \lambda_{2N}$. The 'critical' value $\Omega_R^* = -\Delta$ separating these two regimes reflects the transition of the proton from the surroundings to the states where the proton is shared by the chain water molecules, which corresponds to the protonation chemical reaction. Figure 2 shows the variation of the average occupancies of proton sites with Ω_R for the chains containing $N = 2$ and 3 H bonds. For low temperatures (see the case $T = 30$ K) the boundary proton occupancies $\langle n_{1a}\rangle = \langle n_{Nb}\rangle$ drop drastically to zero at $\Omega_R = \Omega_R^*$, whereas the occupation numbers of the central positions $\langle n_{1b}\rangle = \cdots = \langle n_{Na}\rangle$ increase up to the value $\frac{1}{2(N-1)}$, reflecting the redistribution of the collectivized proton between the inner sites in the wire. It should be noted here that Ω_R^* reflects the change of the ground state of the system and is determined as the solution of the equation $\lambda_{1,2} = \lambda_{4,6,\ldots,2N}$ at $E = 0$ which does not depend on temperature. However, as for all statistical averages, the average proton occupancies (for example, of the states $|1, b\rangle = \frac{1}{\sqrt{2}}(\widetilde{|1, b\rangle} + \widetilde{|2, a\rangle})$ and $|2, a\rangle = \frac{1}{\sqrt{2}}(-\widetilde{|1, b\rangle} + \widetilde{|2, a\rangle})$, where $\widetilde{|1, b\rangle}$ and $\widetilde{|2, a\rangle}$ are the diagonalized states corresponding to λ_4 and λ_3 respectively), are temperature dependent. Thus the value of $\Omega_R^*(T) \approx -\Delta + kT\ln 2$ where $\langle n_{1a}\rangle = \langle n_{2b}\rangle$, for $T \neq 0$ is not equal to Ω_R^* (see figure 2, case $T = 300$ K). This difference shows that the inner proton states (10) are stabilized already at lower $\Omega_R = \Omega_R^* < \Omega_R^*(T)$, although the occupancies of the inner positions at $\Omega_R = \Omega_R^*$ are still slightly lower than of the outer due to the temperature-induced fluctuations. As $T \to 0$, the fluctuations decrease and $\Omega_R^*(T) \to \Omega_R^*$.

The effect of the proton localization inside the chain is supported by the results reported in [27, 31], showing that in H-bonded finite chains the excess charge is best solvated by the central H bonds. However, as turns out from the analysis presented above, the effect of proton localization is drastically influenced by the competition between two different tendencies:

(i) for small Ω_R, the proton is located near the surrounding/wire interface due to the nonzero protonation barrier Δ;
(ii) to overcome the barrier between the surroundings and the wire, the reorientation energy should be sufficiently large ($\Omega_R > -\Delta$) in order to stabilize the inner proton configurations.

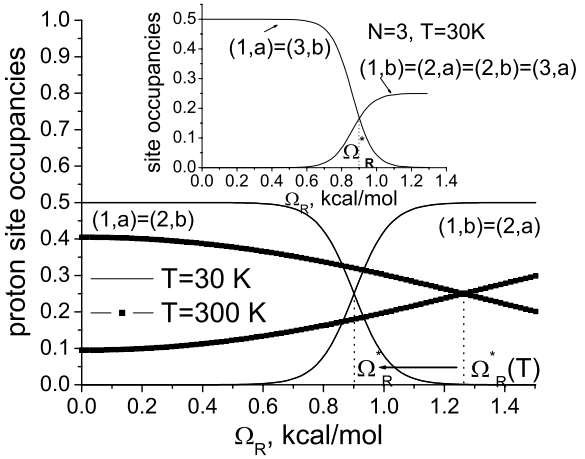

Figure 2. Proton site occupancies for different reorientation energies Ω_R in the chain with two hydrogen bonds containing one excess proton. The inset shows the redistribution of proton charge in the chain with $N = 3$ H bonds.

These conclusions show that, in general, these two different factors (interface barrier and orientations) can be rate limiting for the charge translocation and proton conductivity of the wire. As was shown in [32], the effective reorientation barrier can be influenced by a temperature factor or applied voltage (for example, the reorientation rate of the wire decreases exponentially with T decrease). Thus, one can also expect that the increase of the temperature can result in a lower orientation barrier Ω_R, delocalization of the proton and consequently higher values for the proton conductivity through the channel. However, more detailed theoretical analysis is needed to understand better the role of the interface in the behaviour of the conductivity.

We turn now to an analysis of the proton translocation directed by the external field (the case $E \neq 0$). Figure 3 shows the field dependences of P and $\langle n_{lv} \rangle$ for the chain containing $N = 2$ H bonds. We note that the behaviour in the first small- and in the second large-Ω_R regime differs drastically. In the small-Ω_R regime the polarization increases smoothly with E finally approaching its maximal saturation value $P_{max} = \mu_r + \mu_{ab}$ (figure 3(a), inset). In contrast to this, in the large-Ω_R regime the field dependence is rather nontrivial: first, for $E < E_{thresh}$, P changes very slowly, and then, at $E \sim E_{thresh}$, a strong increase of P to $P = P_{max}$ is observed in figure 3(a). This rapid steplike change of the proton polarization reflects the threshold-type effect where the threshold electric field value at low T is given by

$$E_{thresh} = \frac{\Delta \cdot \mu_H + \sqrt{\Delta^2 \mu_r^2 + \Omega_r^2(\mu_H^2 - \mu_r^2)}}{\mu_H^2 - \mu_r^2}, \qquad (\mu_H = \mu_r + \mu_{ab}) \qquad (11)$$

and does not depend on the chain size N ($E_{thresh} \approx 0.15 \times 10^{-7}$ V cm^{-1} for the chains with $N = 2$ as can be observed in figure 3(a)). As we see in figure 3(b), the proton charge translocation under the influence of the field in this case proceeds not smoothly, but has a steplike character. As results from (11), the threshold value E_{thresh} (which is needed to overcome a barrier for pumping between the inner localized states (10) and the boundary state $|00\ldots01\rangle$ in the direction of field) increases for larger Ω_R (figure 3(a), the cases with $\Omega_R = 1.5$ and 2.15 kcal mol^{-1}). This implies that the conductivity of protonated chains can drop with an increasing Ω_R which can occur in a system for example due to the

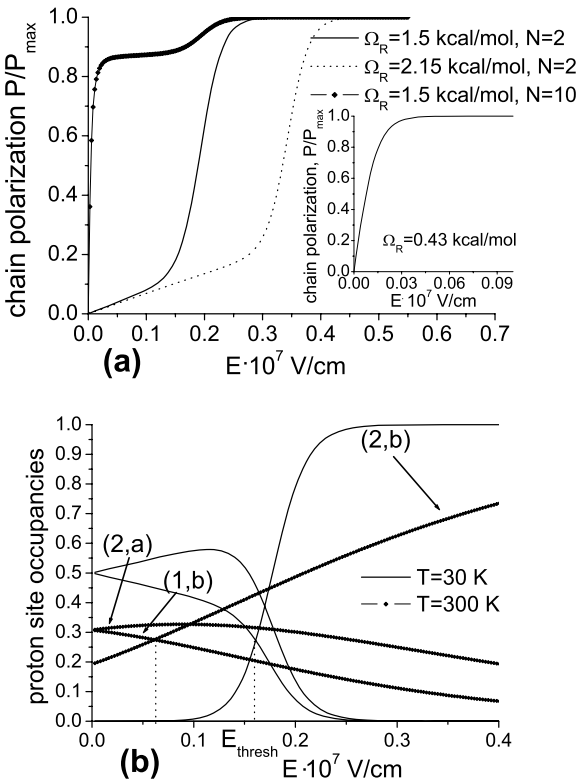

Figure 3. (a) Proton polarization versus electric field in the small-Ω_R (shown in the inset) and large-Ω_R regimes for $T = 30$ K, and (b) average site occupancies versus E in the chain containing $N = 2$ hydrogen bonds and $n = 1$ proton for $\Omega_R = 1.5$ kcal mol^{-1} and for different temperatures.

temperature-induced fluctuations of Ω_R. However, as was shown in [32], the reorientation rate increases at increased voltage, which corresponds in our case to the smaller values of Ω_R for $E \neq 0$. Thus, we can expect that the external field-induced lowering of the orientation barrier for the proton translocation results in the increase of the proton conductivity in the wire.

The drastic change of P at $E = E_{thresh}$ leads to a strong qualitative difference in the temperature shapes of the polarization profiles shown in figure 4(a) for the large-Ω_R regime. For $E < E_{thresh}$ and $\Omega_R > \Omega_R^*$, the excess proton is located in the central sites, and the increase of T results in a disorder-induced transfer of the proton from the inner positions to the chain boundary giving the increase of P at 300 K as compared to 50 K (figure 4(a), cases $E = 0.02 \times 10^7$ and 0.1×10^7 V cm^{-1}). As the proton is located in the outer state $|00\ldots01\rangle$ for $E > E_{thresh}$ (corresponding to $P = 1$ for $T \to 0$), the dominant effect of T in this case is the disorder-induced proton redistribution between all sites in the chain leading to the lowering of total polarization (figure 4(a)), cases $E = 0.2 \times 10^7$ and 0.3×10^7 V cm^{-1}). The profiles of the polarization for Ω_R below Ω_R^* shown in figure 4(b) appear to be very similar to the high-field profiles in figure 4(a). Since for $\Omega_R < \Omega_R^*$ the proton is located in the outer states (9) near the chain boundary already at low E, the increase of T suppresses the polarization due to the increasing proton disorder.

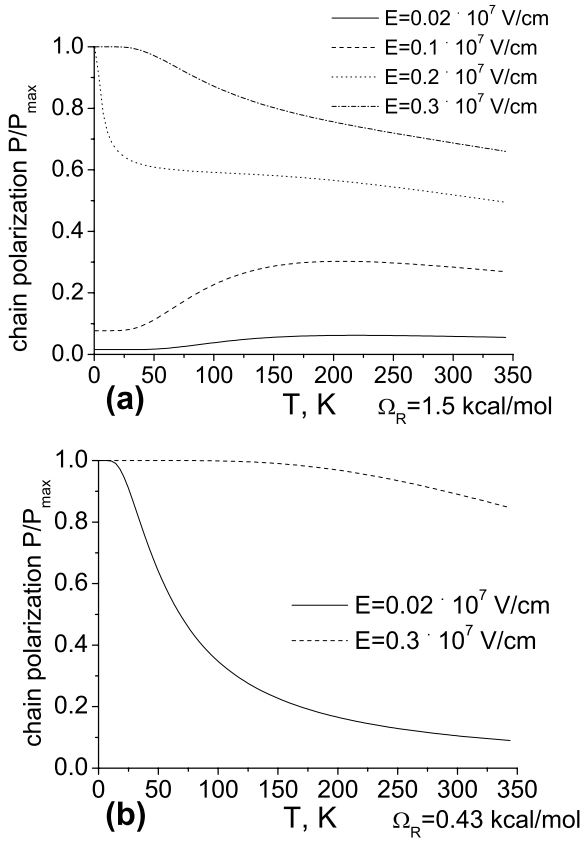

Figure 4. Proton polarization versus temperature (a) in the large-Ω_R regime and (b) in the small-Ω_R regime for different values of applied electric field E.

4. Role of proton–proton correlations

In order to examine the influence of proton correlations, we consider next the translocation of two excess protons in the wire which is described by the part H^2 of the total energy (A.4). Since the presence of two protons in the wire may lead to the formation of a Bjerrum D-defect, the energy H^2 for the chain with $N = 2$ H bonds given by the expression (A.6) contains the terms with the energy U of the repulsion between two nearest-neighbouring protons.

Analogously to the one-proton wire, we analyse first the behaviour of the chain without the electric field. For $N = 2$ and $\Omega_T \approx 0$ the energy levels found from (A.6) have the form

$$\begin{aligned} &\lambda_{1,2} = \tfrac{1}{2}(U \pm q_-) + \mu_H E, \\ &\lambda_3 = \Delta, \\ &\lambda_4 = -\Delta + J, \\ &\lambda_{5,6} = \tfrac{1}{2}(U \pm q_+) - \mu_H E, \qquad \left(q_\pm = \sqrt{(U \mp 2\mu_r E)^2 + 4\Omega_R^2}\right) \end{aligned} \tag{12}$$

and correspond to the following states of the wire:

$$
\begin{aligned}
|\tilde{1}\rangle &= \frac{p_-}{\sqrt{\Omega_R^2 + p_-^2}}|6\rangle + \frac{\Omega_R}{\sqrt{\Omega_R^2 + p_-^2}}|7\rangle,\\
|\tilde{2}\rangle &= \frac{\Omega_R}{\sqrt{\Omega_R^2 + p_-^2}}|6\rangle - \frac{p_-}{\sqrt{\Omega_R^2 + p_-^2}}|7\rangle,\\
|\tilde{3}\rangle &= |8\rangle,\\
|\tilde{4}\rangle &= |9\rangle,\\
|\tilde{5}\rangle &= \frac{\Omega_R}{\sqrt{\Omega_R^2 + p_+^2}}|10\rangle + \frac{p_+}{\sqrt{\Omega_R^2 + p_+^2}}|11\rangle,\\
|\tilde{6}\rangle &= -\frac{p_+}{\sqrt{\Omega_R^2 + p_+^2}}|10\rangle + \frac{\Omega_R}{\sqrt{\Omega_R^2 + p_+^2}}|11\rangle
\end{aligned}
\tag{13}
$$

with $p_\pm = \frac{1}{2}(U \pm q_\pm) \mp \mu_r E$.

To study the influence of Ω_R, we analyse (12) and (13) for $E = 0$ assuming $J \gg U$ and neglecting in this way the formation of ionic defects described by the configuration $|9\rangle = |0110\rangle$. Similarly to the one-proton wire, the two different regimes can exist in the system depending on the value of the reorientation energy. In the first *small-Ω_R regime* (for $\Omega_R < \Omega_R^{*(2)} = \sqrt{\Delta^2 - U\Delta}$), each proton is located near the outer molecular group and the state $|8\rangle = |1001\rangle$ has the lowest energy $\lambda_3 = \Delta$. As Ω_R increases and approaches the 'critical' value $\Omega_R^{*(2)}$, the transition to the *large-Ω_R regime* occurs. In this regime (for $\Omega_R > \Omega_R^{*(2)}$) the lowest energy levels $\lambda_2 = \lambda_6 = \frac{1}{2}(U - q)$ ($q = q_+(E = 0) = q_-(E = 0)$) correspond to the states $|\tilde{2}\rangle$ and $|\tilde{6}\rangle$ in (13), with one proton located in the interior of the wire. However, in contrast to section 3, the transition between these two regimes is U dependent, because $\Omega_R^{*(2)}$ contains the energy of the D-defect U. Figure 5(a) shows the variation of the proton occupation numbers $\langle n_{lv}\rangle$ with Ω_R for $U = 9.4$ and 1.9 kcal mol^{-1} (plotted in the inset). The 'critical' value $\Omega_R^{*(2)} \approx 3$ kcal mol^{-1} for the repulsion energy $U = 9.4$ kcal mol^{-1} is larger as compared with $\Omega_R^{*(2)} \approx 1.5$ kcal mol^{-1} for $U = 1.9$ kcal mol^{-1}. So far as the repulsion energy U is significant, $\Omega_R^{*(2)} > \Omega_R^*$. However, as $U \to 0$, $\Omega_R^{*(2)}$ approaches the 'critical' value Ω_R^* for the one-proton case. As we can see from (13) and (A.1), the ground states $|\tilde{2}\rangle$ and $|\tilde{6}\rangle$ in the large-Ω_R regime are represented by the superpositions of the normal configurations $|7\rangle$ and $|10\rangle$ and the states $|6\rangle$ and $|11\rangle$ containing the D-defect. Thus the transitions to the large-Ω_R regime stabilize D-defects inside the chain. The formation of the D-defect states is clearly observed in figure 5(a) where the occupation numbers of the D-defect states $|6\rangle$ and $|11\rangle$ significantly increase for $\Omega_R > \Omega_R^{*(2)}$.

Analogously to the one-proton case, the temperature fluctuations lead to the slight temperature-induced increase of the value $\Omega_R^{*(2)}(T)$ (corresponding to $n_{\tilde{3}} = n_{\tilde{2}} = n_{\tilde{6}}$), as compared to $\Omega_R^{*(2)}$ where the states $|\tilde{2}\rangle$ and $|\tilde{6}\rangle$ are already stabilized. In fact, for $\Omega_R > \Omega_R^{*(2)}(T)$ the states corresponding to protonated chains with significant concentration of D-defects prevail ($n_{\tilde{2}} = n_{\tilde{6}} > n_{\tilde{3}}$), whereas the states with the protons located at the boundaries in the surroundings dominate for $\Omega_R < \Omega_R^{*(2)}(T)$ ($n_{\tilde{3}} > n_{\tilde{2}} = n_{\tilde{6}}$). For small $\Omega_R \ll U$, $\Omega_R^{*(2)}$ can be given by

$$
(\Omega_R^{*(2)}(T))^2 = \frac{\Omega_R^{*(2)}}{2}\left[1 + \sqrt{1 + \frac{8kTU^2(U/2 - \Delta)}{\Delta^2 - U\Delta}}\right]. \tag{14}
$$

Since the line $\Omega_R^{*(2)}(T)$ found from (14) is tilted with respect to T in the state diagrams (T, $\Omega_R^{*(2)}(T)$) (figure 5(b)), the effect of temperature for the chain in the large-Ω_R regime

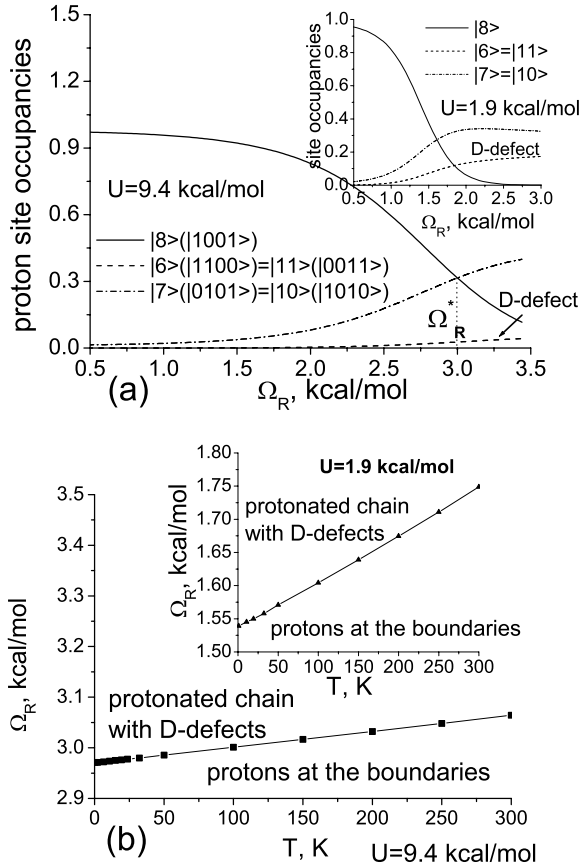

Figure 5. (a) Proton charge distribution versus Ω_R in the H-bonded chain ($N = 2$) containing two protons ($n = 2$) for $T = 100$ K. The inset shows the variation of proton charge with Ω_R for $U = 1.9$ kcal mol^{-1}. (b) State diagrams (T, Ω_R) for $N = 2$, $n = 2$ indicating the regions of stability of the protonated chain with a D-defect and the states with the protons localized at the boundaries. The inset shows the state diagram for lower $U = 1.9$ kcal mol^{-1}.

is crucial: with increasing T, the temperature fluctuations can destroy the D-defects and redistribute the proton charge between the other chain sites. See for example the case of $\Omega_R^{*(2)}(T) = 3$ and $U = 9.4$ kcal mol^{-1} plotted in figure 5(b) where the D-defects annihilate at $T \approx 100$ K.

As $U \to \infty$, the weight constants for the D-defect states in (13) become smaller: $\frac{\Omega_R}{\sqrt{\Omega_R^2+p_\pm^2}} = \frac{\Omega_R}{\sqrt{\Omega_R^2+\frac{1}{4}(U\pm q)^2}} \to 0$. Thus, the contribution of the D-defect-states to the stable wire configuration goes down as $\frac{1}{U}$ for the stronger proton repulsion U (see for the comparison $\langle n_6\rangle = \langle n_{11}\rangle$ for different U plotted in figure 5(a)).

The fact that the variation of temperature can lead to formation or annihilation of the D-defects is also observed in the T-dependence of the proton polarization. Note that especially for weak external field E, the behaviour of $P(T)$ in the small-Ω_R (figure 6(a), $E = 0.4 \times 10^7$ V cm^{-1}) and in the large-Ω_R regime (figure 6(b), $E = 0.1 \times 10^7$ V cm^{-1}) is drastically different. In the first case, at low T, the predominantly occupied symmetric ground state $|10\ldots01\rangle$ has the total polarization $P = 0$. However, with T increasing, protons tend

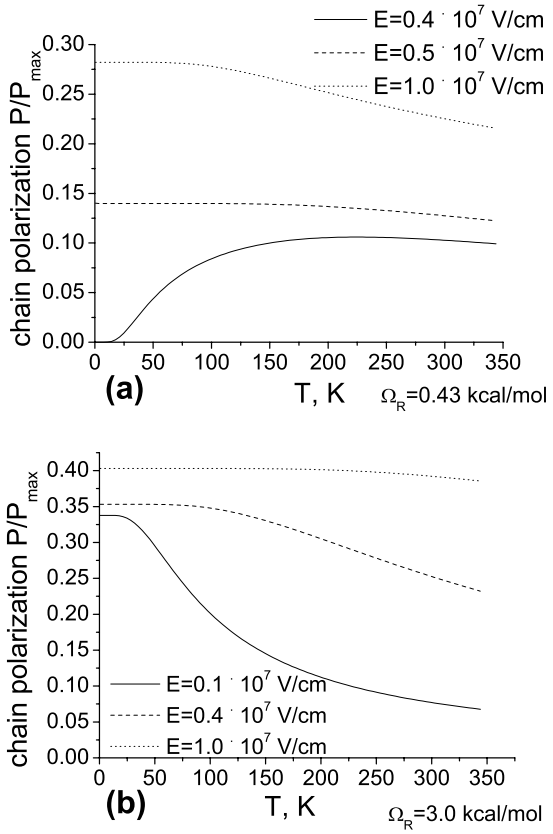

Figure 6. Proton polarization in the chain with $N = 2$ H bonds and $n = 2$ protons versus temperature (a) in the small-Ω_R regime and (b) in the large-Ω_R regime for different values of applied electric field E.

to occupy the excited states with non-symmetric charge distribution that results in an increase of P. Figure 7(a) demonstrates that the population of all excited states, in particular those containing D-defects (figure 7(a), inset), grows with T. Although the concentration of the D-defect states $|0011\rangle$ and $|1100\rangle$ is three to four orders lower than that of the normal states (see figure 7(a), inset), it significantly increases up to one to two orders with the temperature increase from 50 to 300 K.

In contrast to this, in the large-Ω_R regime the protons and stable D-defects migrate in the direction of applied field E for $T \to 0$ giving a non-zero P (figure 6(b)). As T increases, the population of the excited non-defect state with the protons redistributed at the boundaries grows (see figure 7(b)) which gives the lower chain polarization. The D-defects, located near the end of the chain for finite E ($|0011\rangle$), are redistributed between other chain positions with T, which is observed in figure 7(b) showing a decrease of $|0011\rangle$—together with a slight increase of the $|1100\rangle$-state population at $T = 300$ K as compared to lower temperatures.

We now study the electric field effect in correlated chains. Figure 8 shows the variation of polarization and redistribution of protons with increasing E. Consider first the small-Ω_R regime. In contrast to the one-proton wire, where the polarization increases smoothly to its maximal value P_{max} (figure 3(a), inset), we observe here two different threshold effects. The first transition from the state $|8\rangle$ of (A.1) (the ground state of the wire in the small-Ω_R regime

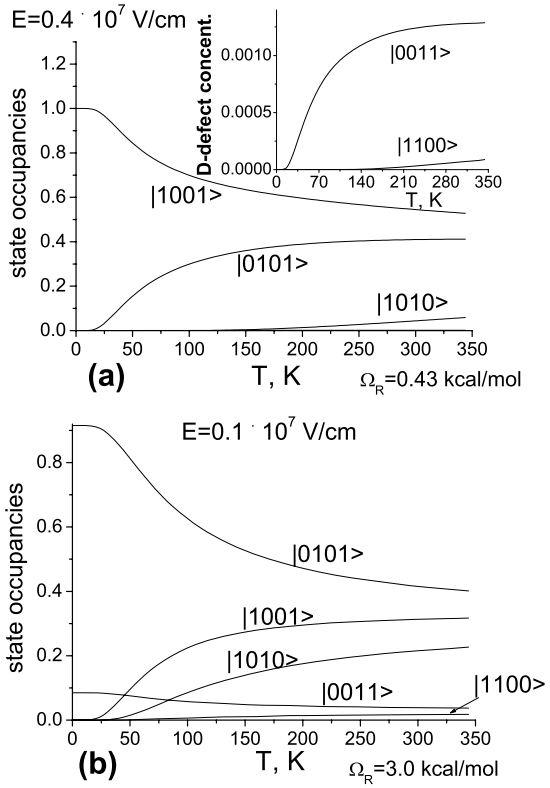

Figure 7. Proton site occupancies in the chain containing $N = 2$ H bonds and $n = 2$ protons versus temperature (a) in the small-Ω_R regime and (b) large-Ω_R regime for low electric field E. The inset shows the concentration of D-defects versus T in the small-Ω_R regime.

at $E = 0$) to the state $|10\rangle$ (where both of the protons are ordered in the right-hand position of each H bond in the direction of the field) occurs at the threshold field value

$$E_1 = \frac{-\Delta}{(N-1)(2\mu_r + \mu_{ab}) - 2\mu_r}. \tag{15}$$

The distribution of the occupation probabilities $\langle n_8 \rangle$ and $\langle n_{10} \rangle$ for the states $|8\rangle$ and $|10\rangle$ is plotted in figure 8(b). We observe at $E = E_1$ the abrupt increase of $\langle n_{10} \rangle$, while at the same field value $\langle n_8 \rangle$ drops to zero. Furthermore, we conclude from (15) that the value E_1 decreases with the number N of the water molecules in the chain. This effect can be observed in figure 9 where the jumps of the polarization are plotted for different N. Finally, for a very long water chain ($N \to \infty$) $E_1 \to 0$. In contrast to the strong N-dependence of E_1, the second threshold effect appears at

$$E_2 = \frac{U}{2\mu_r} \tag{16}$$

essentially due to the proton correlations and does not depend on the chain length. The strong increase of P at $E = E_2$ shown in figures 8(a) and 9 is related to the second drastic redistribution of the proton charge in the wire. As can be observed in figure 8(b), at $E = E_2$ the occupation probability $\langle n_{11} \rangle$ of the D-defect state $|11\rangle$ drastically increases to unity, whereas $\langle n_{10} \rangle$ drops to zero. Thus, as resulted from our model, the formation of the D-defect in external

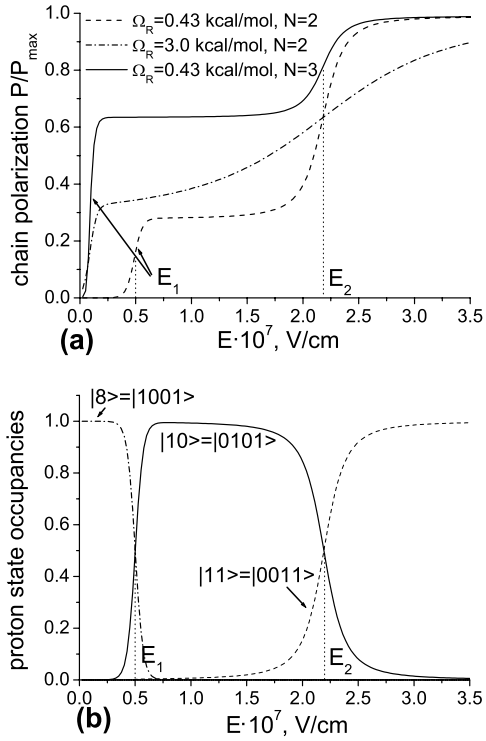

Figure 8. (a) Proton polarization for different Ω_R and (b) average site occupancies for $\Omega_R = 0.43$ kcal mol^{-1} versus electric field E in the chain containing $N = 2$ hydrogen bonds and $n = 2$ protons at $T = 30$ K.

electric field has a steplike character proceeding via the threshold mechanism. In the large-Ω_R regime, where the protons are stabilized at the inner water molecules already at $E = 0$, the first threshold phenomenon at $E = E_1$, observed for the small-Ω_R case, does not occur. However, the transition at $E = E_2$ with the increase of the D-defect concentration appears in this regime similarly to the regime of small Ω_R, that can be observed in the P-profile for $\Omega_R = 3$ kcal mol^{-1} shown in figure 8(a). Note that the effect of the increasing double occupancy due to membrane potentials has been observed in the current/concentration plots in gramicidin channels [32], thus supporting our main conclusions about the role of the external electric field.

The above-discussed formation of the D-defects for $\Omega_R > \Omega_R^*$ in the high electric field results in the increase of P for lower temperatures as shown in figure 6(b). Basically, the essential effect of T observed in the $P(T)$-profiles in figure 6 is the suppression of the total polarization due to proton disorder. However, the shapes of the polarization in figure 6(a) are drastically different for $E < E_1$ and $E > E_2$. For low fields ($E < E_1$) the polarization first increases (reflecting the fluctuation-induced expansion of proton charge from the outer symmetric positions $|10\ldots01\rangle$ with $P = 0$ to the inner positions of the chain accompanied by the formation/annihilation of D-defects), and then smoothly decreases due to the disorder effect. In contrast to this, as the increasing electric field induces the steplike formation of D-defects in the small-Ω_R regime, the temperature behaviour of P in this case is similar to the large-Ω_R case (compare figures 6(a) and (b) with $E = 1 \times 10^7$ V cm^{-1}) showing the smooth disorder-induced decrease of P with T.

We also note that the stable configurations with double proton occupancy require additional reorientation steps for the proton translocation and can result in smaller values for the proton

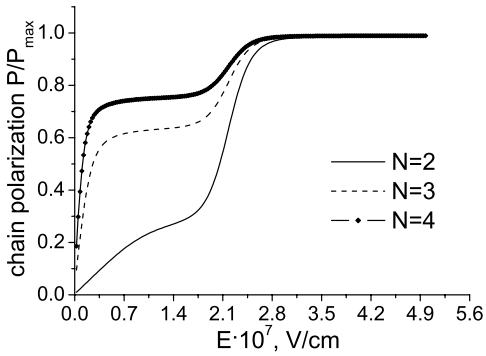

Figure 9. Proton polarization versus E in the chains of different length containing two protons for $\Omega_R = 0.43$ kcal mol^{-1} and $T = 300$ K.

conductivity. This fact has been observed in the measurements of the proton conductance in two different stereoisomers of the gramicidin [6], thus supporting a possibility of stabilization of the D-defect states in proton wires.

5. Summary

In this work we studied the process of proton translocation in 1D chains mimicking protonated water channels embedded in their surroundings. We have analysed the role of the reorientation motion of protons, as well as the effect of electric field and proton correlations on the chain dynamics. We have shown that the increase of the reorientation energy results in the transition to the large-Ω_R regime characterized by the transfer of the proton charge from the surroundings to the inner water molecules in the chain. The process of proton migration along the chain in the external electric field has steplike character leading to the appearance of the electric field threshold-type phenomena with drastic redistribution of proton charge. The correlations between protons in the chain increase the 'critical' reorientation energy Ω_R^* necessary for the transition into the large-Ω_R regime, where the protonated chain contains a finite concentration of Bjerrum defects. The temperature fluctuations induce a slight increase of $\Omega_R^*(T)$ separating the state with the protons located in surroundings near the outer groups, and the protonated state with D-defects. For the correlated chains, this temperature dependence of the 'critical' reorientation energy can lead to the redistribution of proton charge and annihilation of D-defects with increasing T. The electric field applied to the correlated chains induces first the formation of ordered dipole structures for the lower E values, and then, with further E increase, the stabilization of the states with the Bjerrum D-defects.

Generally, the increase of temperature suppresses the total polarization in the chain due to the increasing disorder. However, especially in low electric fields, the shapes of the temperature profiles of the polarization appear to be drastically different in the small- and large-Ω_R regimes demonstrating the complex interplay between the reorientation energy and temperature.

Finally, as follows from our analysis, the following factors strongly influence the formation of Bjerrum defects:

(i) high electric fields can form the defects and pump them in the chain in the direction of field;
(ii) increase of the orientational energy barrier leads to the stabilization of D-defects;
(iii) increase of temperature in the large-Ω_R regime results in the formation/annihilation of

D-defects, whereas for small Ω_R the concentration of D-defects significantly increases by up to one to two orders at room temperatures as compared to low $T \approx 50$ K.

Appendix A. Decomposition of the proton states in the system with $N = 2$ H bonds

We demonstrate below the procedure of mapping in the system with $N = 2$ H-bonds on the multi-site states. For $N = 2$ the basis $|i\rangle$ includes $2^{2N} = 16$ states $|n_{1a}, n_{1b}, n_{2a}, n_{2b}\rangle$:

$$\begin{aligned} &|1\rangle = |0000\rangle, \qquad |2\rangle = |1000\rangle, \qquad |3\rangle = |0100\rangle, \\ &|4\rangle = |0010\rangle, \qquad |5\rangle = |0001\rangle, \qquad |6\rangle = |1100\rangle, \\ &|7\rangle = |1010\rangle, \qquad |8\rangle = |1001\rangle, \qquad |9\rangle = |0110\rangle, \\ &|10\rangle = |0101\rangle, \qquad |11\rangle = |0011\rangle, \ldots, |16\rangle = |1111\rangle. \end{aligned} \tag{A.1}$$

We can derive the relations between $c_{l,v}$ and $X^{ii'} = |i\rangle\langle i'|$:

$$c_{l,v} = \sum_{i,j} \langle i|c_{l,v}|j\rangle X^{ij}, \tag{A.2}$$

where the expectation numbers $\langle i|c_{l,v}|j\rangle$ can be found using the usual antisymmetric rules for Fermi operators [29]. Specifically, for the case $N = 2$ the expressions (A.2) yield

$$\begin{aligned} c_{0,a} &= X^{1,2} + X^{3,6} + X^{4,7} + X^{5,8} + X^{9,12} + X^{10,13} + X^{11,14} + X^{15,16} \\ c_{1,a} &= X^{1,4} - X^{2,7} - X^{3,9} + X^{5,11} + X^{6,12} - X^{8,14} - X^{10,15} + X^{13,16} \\ c_{0,b} &= X^{1,3} - X^{2,6} + X^{4,9} + X^{5,10} - X^{7,12} - X^{8,13} + X^{11,15} - X^{14,16} \\ c_{1,b} &= X^{1,5} - X^{2,8} - X^{3,10} - X^{4,11} + X^{6,13} + X^{7,14} + X^{9,15} - X^{12,16}. \end{aligned} \tag{A.3}$$

Using the relations (A.3) and the fact that $X^{ii'}X^{ll'} = \delta_{i'l}X^{il'}$ (due to the orthogonality of the states $|i\rangle$), we decompose (1)–(5) in terms of $X^{ii'}$ operators into the following five terms:

$$H = H_2^0 \oplus H_2^1 \oplus H_2^2 \oplus H_2^3 \oplus H_2^4, \tag{A.4}$$

where

$$H_2^0 = a_2^0,$$

$$\begin{aligned} H_2^1 = {} & (\Delta + (\mu_r + \mu_{ab})E)X^{2,2} + \mu_r E(X^{3,3} - X^{4,4}) \\ & + (\Delta - (\mu_r + \mu_{ab})E)X^{5,5} + \Omega_T(X^{2,3} + X^{3,2}) \\ & + \Omega_T(X^{4,5} + X^{5,4}) + \Omega_R(X^{3,4} + X^{4,3}) + a_2^1, \end{aligned} \tag{A.5}$$

$$\begin{aligned} H_2^2 = {} & (U + (2\mu_r + \mu_{ab})E)X^{6,6} + \mu_{ab}(X^{7,7} - X^{10,10}) \\ & + \Delta X^{8,8} + (J - \Delta)X^{9,9} + (U - (2\mu_r + \mu_{ab})E)X^{11,11} \\ & + \Omega_T(X^{7,8} + X^{8,7}) + \Omega_T(X^{8,10} + X^{10,8}) + \Omega_T(X^{9,10} + X^{10,9}) \\ & + \Omega_R(X^{6,7} + X^{7,6}) + \Omega_R(X^{10,11} + X^{11,10}) + a_2^2, \end{aligned} \tag{A.6}$$

$$\begin{aligned} H_2^3 = {} & (U + J - \Delta + (\mu_r + \mu_{ab})E)X^{12,12} + (U + \mu_r E)X^{13,13} \\ & + (U - \mu_r E)X^{14,14} + (U + J - \Delta - (\mu_r + \mu_{ab})E)X^{15,15} \\ & + \Omega_T(X^{12,13} + X^{13,12}) + \Omega_T(X^{14,15} + X^{15,14}) \\ & + \Omega_R(X^{13,14} + X^{14,13}) + a_2^3, \end{aligned}$$

$$H_2^4 = (2U + J)X^{16,16} + a_2^4. \tag{A.7}$$

Since the parameter

$$\Delta = (\tilde{w} - \tilde{\varepsilon}) - (\varepsilon - w') \tag{A.8}$$

in (A.5)–(A.7) is the difference between proton configuration energies at the boundary ($l = 1$ or $N + 1$ surrounding molecular groups), and at the inner ($2 < l < N$) water molecule, it describes, in fact, the energy barrier for the protonation of the water chain. For our analysis Δ has key importance, because the other energy constants in (A.5)–(A.7)

$$a_2^0 = a_2^2 - (\tilde{w} - \tilde{\varepsilon}) - (\varepsilon - w'), \qquad a_2^1 = a_2^2 - (\tilde{w} - \tilde{\varepsilon}),$$
$$a_2^3 = a_2^2 + (\tilde{w} - \tilde{\varepsilon}), \qquad a_2^4 = a_2^2 + (\tilde{w} - \tilde{\varepsilon}) + (\varepsilon - w'),$$
$$a_2^2 = \tilde{w} + \tilde{\varepsilon} + \varepsilon$$

which appear due to the boundary effects, are independent of the proton location in the wire and thus do not influence the statistical characteristics like (6).

In a similar way the energy (1)–(5) can be rewritten for the systems with any finite value of N.

References

[1] Gennis R B 1989 *Biomembranes: Molecular Structure and Functions* (New York: Springer) p 235
[2] Lanyi J K and Pohorille A 2001 *Trends Biotechnol.* **19** 140
[3] Stoeckenius W, Lozier R H and Bogomolni R A 1979 *Biochim. Biophys. Acta* **505** 215
[4] Nagle J F and Mille M 1981 *J. Chem. Phys.* **74** 1367
[5] Levitt D G, Elias S R and Hautman J M 1978 *Biochim. Biophys. Acta* **512** 436
[6] Cukierman S 2000 *Biophys. J.* **78** 1825
[7] Chen M S, Onsager L, Bonner J and Nagle J 1974 *J. Chem. Phys.* **60** 405
[8] Bjerrum N 1951 *K. Danske Vidensk. Selsk. Skr.* **27** 1
[9] Akeson M and Deamer D W 1991 *Biophys. J.* **60** 101
[10] Nagle J F, Mille M and Morowitz H J 1980 *J. Chem. Phys.* **72** 3959
[11] Chernyshev A and Cukierman S 2002 *Biophys. J.* **82** 182
[12] Eisenberg D and Kauzmann W 1969 *The Structure and Properties of Water* (Oxford: Oxford University Press)
[13] de Godoy C M G and Cukierman S 2001 *Biophys. J.* **81** 1430
[14] Pomès R and Roux B 1998 *Biophys. J.* **75** 33
[15] Savin A V and Zolotaryuk A V 1991 *Phys. Rev.* A **44** 8167
[16] Zolotaryuk A V, Savin A V and Economou E N 1994 *Phys. Rev. Lett.* **73** 2871
[17] Tuckerman M, Laasonen K, Sprik M and Parrinello M 1995 *J. Chem. Phys.* **103** 150
[18] Marx D, Tuckerman M, Hutter J and Parrinello M 1999 *Nature* **397** 601
[19] Schumaker M F, Pomès R and Roux B 2000 *Biophys. J.* **79** 2840
[20] Schumaker M F, Pomès R and Roux B 2001 *Biophys. J.* **80** 12
[21] Davydov A S 1982 *Biology and Quantum Mechanics* (Oxford: Pergamon) p 25
[22] Stasyuk I V, Ivankiv O L and Pavlenko N 1997 *J. Phys. Stud.* **1** 418
[23] Pavlenko N 2000 *Phys. Rev.* B **61** 4988
[24] Pavlenko N 2000 *J. Chem. Phys.* **112** 8637
[25] Pavlenko N 2000 *Phys. Status Solidi* b **218** 295
[26] Pavlenko N I and Stasyuk I 2001 *J. Phys.: Condens. Matter* **13** 4081
[27] Pomès R 1996 *J. Phys. Chem.* **100** 2519
[28] Hassan R and Campbell E 1992 *J. Chem. Phys.* **97** 4326
[29] Davydov A S 1965 *Quantum Mechanics* (Oxford: Pergamon)
[30] Rao C N R 1972 Theory of hydrogen bonding in water *Water: a Comprehensive Treatise* vol 1 (New York: Plenum)
[31] Pomès R 1999 *Isr. J. Chem.* **39** 387
[32] Phillips L R, Cole C D, Hendershot R J, Cotten M, Cross T A and Busath D D 1999 *Biophys. J.* **77** 2492